Journal of Pharmaceutical, Chemical and Biological Sciences
ISSN: 2348-7658
CODEN: JPCBBG
Impact Factor (GIF): 0.701
Impact Factor (SJIF): 3.905
June- August 2017; 5(2):133- 146
Published on: 27 August 2017

Research Article

New Green Solvent Interfacial Polymerization Method for Preparation of Nanostructured Polyaniline Composite Photocatalysts and Their Efficient Phenol Degradation With/Without Fenton's Reagent

P. Rajesh Anantha Selvan[1], E. Subramanian[2*], R. Murugesan[3]

[1]Department of Chemistry, St. John's College, Palayamkottai, Tirunelveli-627 002, Tamil Nadu, India.
[2]Department of Chemistry, Manonmaniam Sundaranar University, Tirunelveli-627 012, Tamil Nadu, India
[3]Department of Chemistry, TDMNS College, T. Kallikulam, Tirunelveli-627 113, Tamil Nadu, India

***Corresponding Author:** E. Subramanian, Department of Chemistry, Manonmaniam Sundaranar University, Tirunelveli-627 012, Tamil Nadu, India

Received: 10 July 2017 **Revised:** 27 July 2017 **Accepted:** 02 August 2017

ABSTRACT

Photosensitizer functionality of polyaniline (PANI) and heterogeneous catalysis of phosphotungstic acid PTA have been combined with soft template, poly(vinylpyyrolidone) PVP. By green interfacial polymerization method using coconut oil as the organic phase, the following four materials viz., PANI, PANI-PVP, PANI-PTA and PANI-PTA-PVP were synthesized. UV-vis, FTIR, XRD and SEM showed the interaction of PANI with other components. SEM revealed nanosticks/nanorods for PANI-PVP and surface-projected nanofriges/nanobristles structures on micron-size spherical particles for PANI-PTA and PANI-PTA-PVP composites. The photolysis was carried out using Haber inner irradiation type photoreactor under visible light from 150 W tungsten halogen lamp. The optimal condition for maximum degradation of phenol was: catalyst dosage of 0.50 g/L; initial phenol concentration of 50 mg/L; pH of 4.0; H_2O_2 of 2 mL and constant air flow. New Fenton's reagent modified photocatalysts viz., PANI, PANI-PVP, PANI-PTA and PANI-PTA-PVP at optimal condition exhibited the phenol degradation of 7.4, 13.1, 61.2 and 91.4 % respectively. At optimal condition without Fenton's reagent but with 2 mL H_2O_2, all the catalysts exhibited a slightly lesser value, e.g., PANI-PTA-PVP - 86.2 %. Thus the new green solvent interfacial method produced nanostructured PANI composite photocatalysts with high efficiency in phenol photodegradation.

Keyword: Polyaniline; interfacial polymerization; phosphotungstic acid dopant; phenol photodegradation; fenton's reagent.

INTRODUCTION

Phenolic compounds are present in natural and synthetic sources, and are detected in the effluents of various industries including oil refineries, cocking processes, coal processing, resin manufacturing, wood products, pharmaceutical, plastics, paint, paper as well as pesticide industries. Phenol causes dangerous health effects [1]. Conventional methods such as chemical oxidative degradation [2], catalytic oxidation [3], biodegradation [4], solid-phase extraction [5], liquid-liquid extraction [6], adsorption [7] and many other technologies are used to remove phenol from aqueous solutions.

Many processes such as Fenton's reagent processes [8], ultraviolet (UV)-based degradation [9], photocatalytic redox reaction [10], supercritical water oxidation [11], sonolysis [12] and electron beams [13] come under advanced oxidation processes (AOPs). Advanced oxidation processes are water treatment processes which involve the generation of highly reactive hydroxyl radicals [14], which rapidly and non-selectively oxidize a broad range of organic pollutants inducing phenols. Hydroxyl radicals are generated through different combinations of oxidants of hybrid materials. In this study, visible light photocatalytic degradation of phenol has been examined in the presence of polyaniline (PANI) composite photocatalyst being modified with Fenton's reagent.

The present work involves the preparation of PANI and its heteropoly acid (HPA) composites by green synthesis of interfacial polymerization method [15] in which aniline is polymerized to PANI at the interface of two immiscible liquids and Poly(vinly pyrrolidone) (PVP) is used as co-dopant as well as soft template [16] during composite preparation. Nowadays, special attention is given to the use of vegetable oil due to its biodegradation nature [17] and reduction in particle size [18]. Hence, in the present work vegetable oil, coconut oil is used as the organic phase which contains aniline. The aqueous phase contains heteropoly acid-phosphotungstic acid (PTA) without/with the soft template, PVP. Thus, in a green way the interfacial polymerization is performed to synthesize four catalysts, PANI, PANI-PVP, PANI-PTA and PANI-PTA-PVP. The decomposition of phenol by using these Fenton's reagent modified photocatalysts is studied after varying experimental parameters such as initial phenol concentration, pH and dose of catalyst.

MATERIALS AND METHODS

Materials

Phosphotugstic acid was obtained from Sigma-Aldrich and used without purification. Aniline from Aldrich, was distilled prior to use. Water was used after two distillations (DDW). Phenol, Con. HCl, PVP, N-methylpyrrollidone (NMP), hydrogen peroxide and acetone were obtained from Merck. Coconut oil was of commercially pure grade. Phenol dissolved in DD water was stored in amber colour bottle. Ferrous sulphate, sodium carbonate and Folin-phenol reagent were obtained from Spectrum Chemicals for usage.

Synthesis of PANI materials

PANI was synthesized by green interfacial polymerization method [15] using coconut oil as the organic phase and H_2O_2 as the oxidant. Aqueous solution of 2 mL H_2O_2, 2 mL Con. HCl and 96 mL DDW was poured into a 250 mL separatory funnel. For the composite preparation the aqueous phase with PTA or PVP was taken in a beaker and it was sonicated initially. 2 mL aniline monomer was dissolved in 25 mL coconut oil to form the organic phase and the same was carefully added to the aqueous phase to produce a clear interface of aqueous-organic solutions in the separatory funnel. The polymerization of aniline occurred at the interface. The reaction mixture was left undisturbed for four days for the completion of polymerization reaction. The upper organic phase was carefully removed and the lower phase containing PANI mixture was transferred into a beaker. The solid polymer mass formed was filtered, washed several times with 0.1 M HCl, DDW and acetone until the washings became colourless. The PANI and its composites samples were dried in an air oven at 110°C for 6 h, ground into fine powder and stored in air tight polythene packets. Similarly PANI–PTA and PANI-PVP samples were also prepared with 5 mM PTA and with 10 mM PVP respectively. The ternary PANI–PTA-PVP composite was green synthesized by adopting the same procedure as above with both 5 mM PTA and 10 mM PVP.

Characterization

The UV-vis absorption spectra of all the PANI samples dissolved in NMP solvent were recorded with a Perkin Elmer UV-vis spectrophotometer (Lambda 25 model) in matched 1cm quartz cuvettes in the range of 330 nm to 1100 nm. FTIR spectra (in KBr pellets) were recorded on a JASCO FTIR - 410 spectrophotometer in the wavenumber region 4000-400 cm^{-1}. Powder X-ray diffraction patterns of PANI and its composites samples were performed using a Shimadzu XRD 6000 X-ray diffractometer with Cu-Kα radiation source (λ = 1.54 Å) operated at 40 kV and 30 mA in the 2θ range 10 - 90° at the scan speed of 10.0° per minute. The surface morphologies of PANI and its composites

samples were observed using JEOL JSM-6390 Scanning Electron Microscope (SEM) operating at 20 kV, after coating the samples with platinum for 45 s using JEOL JFC-1600 auto-fine coater with sputtering technique.

Photocatalysis

All photocatalytic experiments were carried out in a Haber inner irradiation type photoreactor model HIPR-LC-150 with 150 W tungsten-halogen lamp and light intensity = 14.79 mW/cm^2 at 555 nm measured with Kusem–Meco Luxmeter, model KM Lux 200 K. 300 mL phenol solution mixed thoroughly with required quantity of photocatalyst and 2 mL H_2O_2 was shaken for 30 min to reach adsorption/desorption equilibrium in the absence of light. The glass cylindrical flask was covered with aluminum foil during shaking and the course of reaction. The pH was adjusted using 0.1 M HCl or 0.1 M NaOH during the experiments. Air was flown at constant rate into the reaction mixture using air pump. Experiments were carried out at the operating temperature of 28±2°C and atmospheric pressure. The first sample after adsorption equilibrium was taken to determine the initial phenol concentration. After that tungsten lamp was switched on to initiate photocatalysis, 2 mL sample was withdrawn out for every 10 min for an hour and remaining samples were taken at 20 min intervals. After each step, phenol samples were centrifuged and filtered using Whatman filter paper No.1 to remove the suspended solid catalyst.

Phenol concentration was analysed by using Phenol-Folin method [19]. In this method 2 mL phenol aliquot was mixed with 0.5 mL Phenol-Folin reagent and 2 mL sodium carbonate (20 % W/V solution) and diluted to 10 mL using DDW. The mixture was heated in a water bath for one minute to develop a blue colour. After 10 min of incubation, absorbance was measured at λ_{max} = 650 nm. The % photodegradation of phenol was calculated using the following equation (1).

$$\% \text{ Degradation} = (C_0 - C_t)100/ C_0 \quad \text{----------(1)}$$

Where C_0 and C_t are the initial concentration and the concentration of phenol after irradiation time (t) respectively. They were determined by absorbance measurement.

Photodegradation study for the four catalysts PANI, PANI-PVP, PANI-PTA and PANI-PTA-PVP was carried out in light, constant air flow, H_2O_2 2 mL, at initial phenol concentration of 50 mg/L, pH = 4 and dose of catalyst = 0.5 g/L. The above experiment was repeated with Fenton's reagent (0.5 mM Ferrous sulphate and 50 mM or 2 mL H_2O_2) under same reaction condition. Influence of experimental variables like initial phenol concentration, pH, and dose of catalyst on photodegradation of phenol was also investigated.

RESULTS AND DISCUSSION

UV-Vis spectral studies

The UV–vis absorption spectra of PANI and its composite materials in NMP solvent are displayed in Fig.1 and peak values are compiled in Table 1. The spectrum of PANI consists of three major absorption bands. The one around 378 nm is assigned to π-π* transition, second one at 561 nm to band gap absorption of benzenoid rings and the other one around 695 nm is assigned to a charge-transfer exciton-like transition related to the quinonoid unit, which can be used as a measure of the oxidation state of polyaniline [20]. All the three absorption bands of PANI are blue-shifted i.e., shifted to lower wavelength/higher energy in PANI-PVP composite. This spectral shift in PANI-PVP composites proves their mutual interaction [20,21]. In PANI–PTA the absorption peak at 384 nm, is the red-shifted π-π* transition of PANI (Fig. 1c) and its intensity relative to other peaks/bands is many times increased when compared to PANI/PANI-PVP. Further the other two bands of PANI (561 and 695 nm) are blue-shifted (544 and 684 nm) and reduced in intensity. The relative increase in absorbance of π-π* band while the decrease in absorbance of emeraldine base to benzenoid/quinoid ring transition bands (544 and 684 nm bands) definitely indicates a strong interaction between PANI and PTA [22] and also a facilitative conversion of emeraldine base to emeraldine salt through doping with PTA [22]. Similar such spectral result is observed in the case of three component composite PANI-PTA-PVP (Fig. 1d). Nevertheless, there is an explicit change. The π-π* peak of PANI at 378 nm (Table. 1) is split into two peaks of unequal absorbance, one at 376 and another at 405 nm. This split is due to the occurrence of additional charge transfer (CT)

transition between PTA and PANI [23]. This split is very small with almost equal absorbance in PANI-PTA (Fig. 1c) but it is very manifestive and unsymmertical in PANI-PTA-PVP composite. That means PVP enhances this CT transition and by this it implies that electraon transfer from PANI to PTA could be of higher degree in PANI-PTA-PVP than in PANI-PTA. In turn, it implies that the former could be a better photocatalyst than latter.

Table 1: UV-vis spectral and XRD data of PANI and its composites

Sample	UV-vis peaks in NMP solvent (nm)	XRD data		
		2θ (deg)	d value (Å)	Average crystallite size (nm)
PANI	378, 561, 695	24.8	3.57	2.53
PANI-PVP	372, 556 688	19.1	4.64	1.87
PANI-PTA	384, 544, 684	18.9	4.67	1.68
PANI-PTA-PVP	376, 405, 548, 690	26.2	3.38	3.64

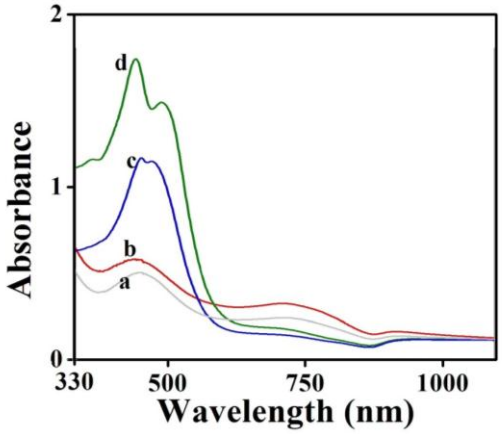

Fig.1: UV-Vis spectra of PANI and its composites in NMP solvent (a) PANI (b) PANI-PVP (c) PANI-PTA and (d) PANI -PTA-PVP

FTIR spectral studies

The FTIR spectra of PANI and its composites are shown in Fig. 2. The characteristic bands of PANI (Fig. 2a), represented by the absorption bands at 1568 cm^{-1} (C=C stretching vibration of the quinoid ring), 1500 cm^{-1} (stretching vibration of C=C of the benzenoid ring), 1444 cm^{-1} (C-N stretching vibration), 1289 cm^{-1} (C-N stretching vibration in quinoid), 1167 cm^{-1} (C-H in-plane bending deformation), 1064 cm^{-1} (C-H in-plane bending) and 784 cm^{-1} (C-H out-plane bending), indicate polymer formation of aniline [20-26]. In PANI – PVP composite the FTIR spectrum (Fig. 2b) is well-resolved and all the peaks have relatively high intensity compared to the spectrum of PANI (Fig. 2a). For example, the two bands at 1572 and 1503 cm^{-1} (quinoid and benzenoid ring stretching in PANI) have relatively high intensity. Also the band at 1304 cm^{-1} assigned to C-N stretching in PVP [16,21] confirms the presence of PVP in the composite. In PANI-PVP composite the peaks shifting at 1572, 1503, 1304, 1133 and 815 cm^{-1} demonstrates clearly the interaction between PANI and PVP [21,27]. In PANI – PTA (Fig. 2c) the characteristic peaks of PANI occur at 1610, 1510, 1307 and 1111 cm^{-1} [20-26] and those of PTA at 968, 883 and 818 cm^{-1} [22,23,26]. The peaks at 1111 cm^{-1} is assigned to a P–O bond, at 968 cm^{-1} to a W = O terminal bond, at 883 cm^{-1} to vertex W–O–W bond and finally at 818 cm^{-1} to a symmetrical stretch W–O–W bond which is combined with C-H out of plane bending in PANI. As in the case of PANI-PVP, here also shifts in peak position and intensity changes are observed in the IR spectra. Thus the presence and interaction of PTA with PANI is confirmed. PANI–PTA–PVP sample (Fig. 2d) has well-

resolved sharp peaks in its IR spectrum. The peaks are slightly shifted to higher wavenumber side indicating the mutual interaction of PVP-PTA and also with PANI.

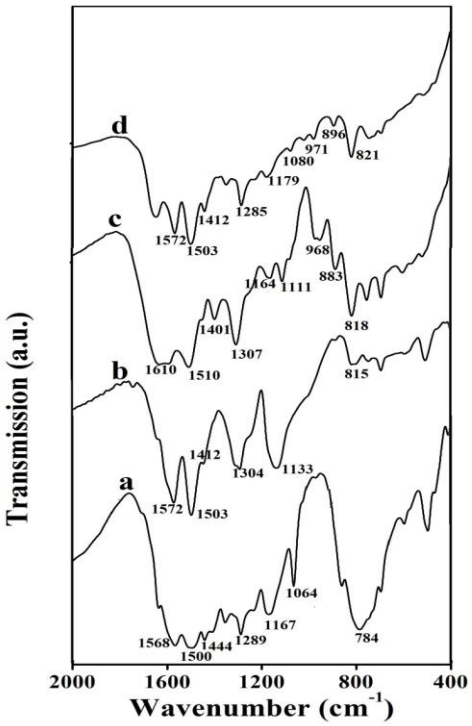

Fig.2: FTIR spectra of PANI and its composites (a) PANI, (b) PANI-PVP, (c) PANI-PTA and (d) PANI-PTA-PVP

XRD studies

Fig. 3 shows XRD patterns of PANI and its composites and the data obtained from these patterns are entered in Table 1. It is discernible from Fig. 3 that the observed peaks of PANI and its composite materials (PANI-PVP and PANI-PTA; Figs. 3b and c) are diffuse and considerably broad and suggest generally amorphous nature. Two broad diffraction peaks are exhibited for PANI at 2θ = 18.6° and 24.8°. These peaks can be attributed to the periodicity parallel and perpendicular to the polymer chains, respectively [21,27]. PANI-PVP shows two peaks, one at 19.1° and another at 24.0°. The peak positions reveals that the first peak is displaced towards the higher angle (lower d-space) and other peak towards lower angle (higher d-space).

PANI–PTA also exhibits broad peaks one at 18.9° and another at 25.4°. The XRD patterns are in good agreement with the literature reports [28,29]. PANI-PTA-PVP exhibits a pattern of completely sharp signals at various 2θ/d values. The maximum intensity peak appears at 26.2°. This sharp multi-signal pattern indicates, beyond any doubt, the presence of crystallinity in PANI-PTA-PVP sample. The soft template PVP and the HPA - PTA mutually interact and also with PANI resulting in the conversion of amorphous PANI into a completely crystalline PANI-PTA-PVP sample. The average crystallite site values determined by Scherrer method are 2.53, 1.87, 1.68 and 3.64 nm for PANI, PANI-PVP, PANI-PTA and PANI–PTA–PVP samples respectively and, therefore these materials have nano-size particles [30]. Thus XRD characterization not only proves the presence of each component but also their interaction and the amorphous/crystalline nature.

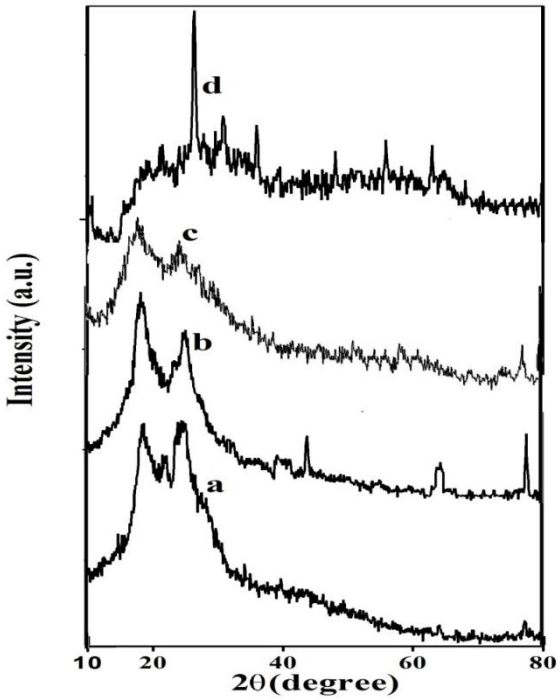

Fig.3: XRD patterns of PANI and its composites (a) PANI (b) PANI-PVP (c) PANI-PTA and (d) PANI-PTA-PVP

SEM studies

SEM pictures of PANI and its composites are shown in Fig.4. PANI has somewhat rough-surfaced, different sized (roughly 2-10 μ) and almost spherically-shaped grains (Fig. 4a). White patches/dots which could be seen on careful view, definitely represent nanospheres or nano rice-like structures of PANI. These spheres have undergone agglomeration into bigger secondary grains mentioned above. PANI-PVP (Fig. 4b) has a characteristically different morphology from others. Nanorods/sticks of few micron length and few hundred nm diameter are clearly visible. In addition, undefined-shaped and sized and smooth surfaced larger flakes are also seen. Undoubtedly, these flakes have been formed by extensive agglomeration [21,27] of these primary nanorods/sticks. The flakes structures are in consistent with very broad and double-humped XRD pattern of PANI-PVP shown in Fig. 3b. PANI-PTA, on the other hand, has a smaller (submicron sized) spherical particles morphology [31]. There is almost uniform size distribution among the spheres and similar to PANI, the particles are slightly rough-surfaced. The three component material PANI-PTA-PVP has a similar morphology (Fig. 4d) of PANI-PTA but the particles are about doubly-sized compared to those of PANI-PTA. This bigger size formation may be due to the agglomeration inducing nature of PVP, as observed in PANI-PVP case with flakes structure. The small degree of crystallinity in PANI-PTA and PANI-PTA-PVP materials as observed form their relatively sharp peaks pattern (Fig. 3c and d), are present in these materials, particularly in their primary fringes/bristles nanostructures (nanocrystalline) projected from the surface of secondary particles/grains.

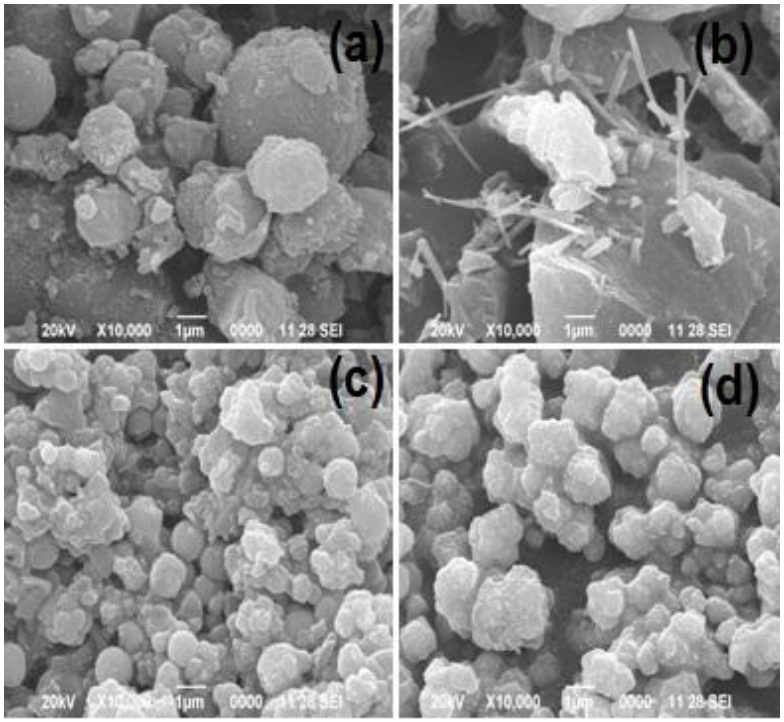

Fig. 4: SEM images of (a) PANI (b) PANI-PVP (c) PANI-PTA and (d) PANI-PTA-PVP

Studies on Photodegradation

The preliminary experiment was performed at the condition of 1) in light, constant air flow, 2) in light, constant air flow and H_2O_2 2 mL, 3) synthesized catalyst under dark condition and air flow, 4) under light, constant air flow and Fenton's reagent (0.5 mM Fe^{2+} and H_2O_2 2 mL; 50 mM) addition at initial phenol concentration of 50 mg/L, pH = 4 and dose of catalyst of 0.5 g/L. These preliminary experiments were performed in order to assess the contribution of individual component to phenol degradation. The results of the above experiments are plotted in Fig. 5. The degradation of phenol in all the preliminary experiments is not significant or is very dismal under light irradiation [32], under light and constant air flow and Fenton's reagent addition. That means without catalyst or without the oxidant H_2O_2 or Fenton reagent phenol decomposition did not take place.

The photocatalytic performance of the four catalysts PANI, PANI-PVP, PANI-PTA and PANI-PTA-PVP was investigated under light and air-flow but without H_2O_2 or Fenton's reagent (Fig. 6). Photocatalytic degradation of 5.3, 9.8, 28.4 and 56.3 % respectively was observed for the four catalysts under light, at constant air flow; [phenol] = 50 mg/L; pH = 4; Temp: 28±2°C; and catalyst dose of 0.50 g/L. Even without H_2O_2, the 3rd and 4th catalysts are able to degrade phenol, of course, to a lesser extent. When the degradation of phenol was studied with constant air flow and H_2O_2 2 mL at the same reaction condition above (Fig. 7) the degradation of 7.4, 19.4, 61.2 and 86.2 % respectively was obtained. Evidently this result demonstrates that these four materials function as photocatalysts and could produce reactive oxygen species like $\cdot OH$, $O_2^{\cdot-}$ etc., with aerial O_2 or H_2O_2. Also addition of PVP and/or PTA to PANI enhances the latter's activity. Particularly, the combination PTA-PVP works better and the resulting catalyst PANI-PTA-PVP exceedingly has a higher efficiency than others.

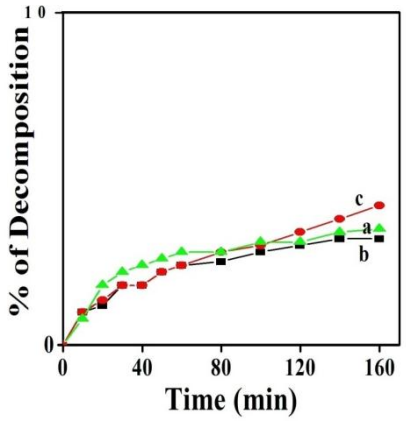

Fig. 5. Photocatalytic degradation of phenol (a) in dark in the presence of PANI and air flow (without oxidant H_2O_2) (b) in light, constant air flow and H_2O_2 2 mL (without catalyst PANI) (c) in light, constant air flow and Fenton's reagent

Effect of types of catalyst with Fenton's reagent addition

After studying the photodegradation of phenol with the four catalysts, involving H_2O_2, it was of our interest to know the influence of Fenton's reagent on phenol degradation. Hence experiments were conducted with the Fenton's reagent of 0.5 mM Fe^{2+} ($FeSO_4.5H_2O$) and 50 mM H_2O_2 (2 mL H_2O_2) in the molar stoichiometric ratio of 1:100 (Fe^{2+}: H_2O_2). The results are displayed in Fig. 8. As for PANI composite, the highest photodegradation of about 91.4 % for phenol is achieved with PANI–PTA–PVP along with Fenton's reagent [33]. This is higher than PANI, PANI–PVP and PANI–PTA which exhibit decomposition of 17.4, 23.2 and 61.2 % respectively. Considering the results of efficiency of the four catalysts in phenol degradation with H_2O_2 (Fig. 7) and with Fenton's reagent (Fig. 8), it is discernible that using Fenton's reagent considerable increase in efficiency (2.5 times) has occurred with PANI only; with PANI-PVP and PANI-PTA-PVP catalysts, only a slight increase in efficiency has resulted in, and with PANI-PTA, surprisingly, the same efficiency (61.2 %) is maintained with Fenton's reagent. The obtained result yields the following inference: when the catalyst (PANI) is unable/ineffective in producing •OH radicals with H_2O_2 alone, Fenton's reagent has greater influence; when the catalyst (PANI-PTA) is fully effective in producing •OH radicals with H_2O_2, Fenton's reagent has no influence and when the catalyst has a small deficiency (PANI-PVP and PANI-PTA-PVP), Fenton's reagent complements it and slightly increases the efficiency. Whatever be the result, since Fenton's reagent exhibits some influence, all the optimization experiments of parameter variables (initial phenol concentration, pH and catalyst dose) involve Fenton's reagent. The following sections present and discuss the results.

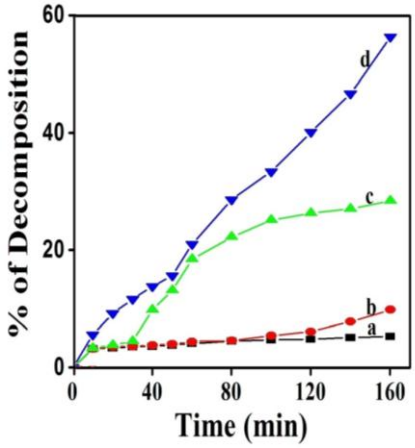

Fig. 6. Photocatalytic performance of (a) PANI (b) PANI- PVP (c) PANI-PTA and (d) PANI-PTA-PVP in phenol degradation Condition: [phenol] = 50 mg/L; pH = 4; Temp = 28±2°C; catalyst dose = 0.5 g/L and constant air flow (no H_2O_2)

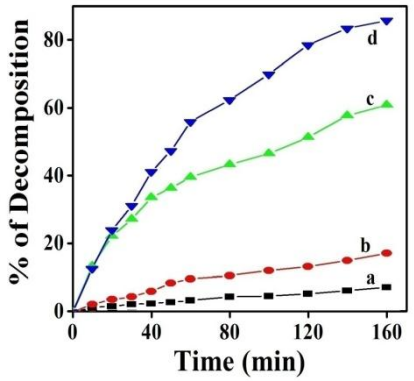

Fig. 7. Photocatalytic performance of (a) PANI (b) PANI- PVP (c) PANI-PTA and (d) PANI-PTA-PVP in phenol degradation. Condition: [phenol] = 50 mg/L; pH = 4; Temp = 28±2°C; and catalyst dose = 0.5 g/L, constant air flow and H_2O_2= 2 mL.

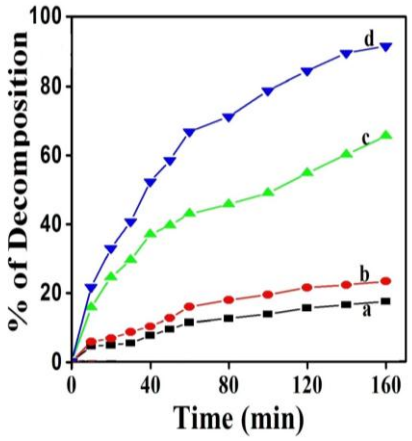

Fig. 8. Photocatalytic performance of (a) PANI (b) PANI-PVP (c) PANI-PTA and (d) PANI–PTA–PVP in phenol degradation with Fenton's reagent
Condition: [phenol] = 50 mg/L; pH = 4; Temp = 28±2°C; catalyst dose = 0.50 g/L; Fenton's reagent (0.5 mM Fe^{2+} and 50 mM 2 mL H_2O_2) and constant air flow

Effect of initial phenol concentration

Fig. 9 shows the effect of initial phenol concentration, with concentration inputs of 10, 30, 50 and 70 mg/L. Degradation of 5.4, 21.4, 45.7 (91.4 %) and 45.1 (64.4 %) mg/L respectively was obtained. As the initial concentration increases, the amount of phenol degraded also increases, having maximum degradation at 50 mg/L (91.4 %) and then it slightly decreases at 70 mg/L. As the initial phenol concentration increases, more and more molecules get adsorbed on the surface of the catalyst and the need of reactive species (•OH and $•O^-_2$) for the degradation of pollutant also increases [34]. However, the formation of •OH and $•O^-_2$ on catalyst surface remains constant for a given light intensity, catalyst amount and duration of irradiation. Hence, when the initial phenol concentration reaches 50 mg/L, saturation in adsorption and reactivity with free radicals also reaches, resulting in maximum degradation; with further increase in concentration, the •OH radicals are inadequate for the pollutant degradation [34-36].

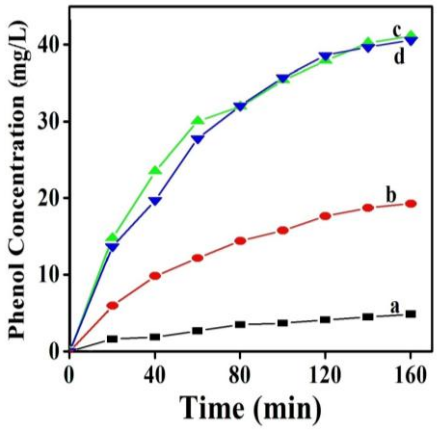

Fig. 9. Effect of initial phenol concentration on its degradation (a) 10 (b) 30 (c) 50 and (d) 70 mg/L .
Condition: pH = 4; Temp = 28±2°C; dose of PANI-PTA-PVP = 0.50 g/L, Fenton's reagent and constant air flow

Effect of pH

pH plays a key role. Because the solution pH directly and indirectly affects the production of hydroxyl radicals and phenol decomposition. The solution with phenol concentration of 50 mg/L was provided at the pH variation of 2, 4, 6, and 8 and the percent of phenol removal was 30.6, 91.4, 36.2 and 16.7 % respectively (Fig.10). According to the results, the maximum efficiency for phenol degradation was achieved at pH = 4. Fenton's reaction will be impeded at upper pH values (6 and 8) due to the creation of Fe^{2+} complexes, sedimentation of iron oxyhydroxides, and decreased oxidation potential of ·OH [37]. The point of zero charge, pH_{zpc} for PANI-PTA-PVP was determined as 6.96, an almost neutral pH. At highly acidic pH 2.0, the surface charge of the catalyst is positive, since H^+ can be attached to aniline group. This is an unfavorable situation. While at pH 8.0, the catalyst surface may be negative. Since pKa of phenol is 11, at higher pHs 6 and 8, the proportion of availability of phenoxide ion will be increasingly higher. Hence there could be electrostatic repulsion between phenoxide and catalyst, which renders phenol adsorption difficult. Altogether pH 4.0 is a conducive condition for maximum adsorption of phenol and is, thus the optimum pH condition. A similar observation has been noted in previous studies [38,39]. Thus at moderate pH value (pH = 4), phenol was degraded larger than at other pHs.

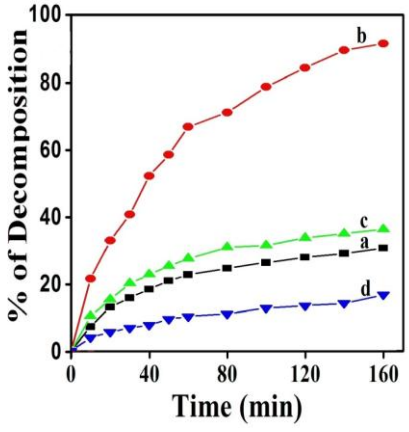

Fig. 10. Effect of pH variation on photodegradation of phenol (a) 2 (b) 4 (c) 6 and (d) 8.
Condition: [phenol] = 50 mg/L; Temp = 28±2°C, Dose of PANI-PTA-PVP = 0.50 g/L, Fenton's reagent and constant air flow

Effect of the dose of catalyst

To determine the effect of catalyst loading, several experiments were conducted at catalyst loading from 0.33 to 0.83 g/L (feed phase pH = 4) at the pollutant concentration of 50 mg/L. Fig. 11 clearly indicates that the increase in amount of catalyst loading increases the % of degradation upto the catalyst amount of 0.5 g/L, (91.4 % degradation). Above this catalyst loading, the turbidity of the solution increases and light starts getting scattered, hence reducing the optical path [34-36]. That is further increase in photocatalyst dosage of 0.66 g/L or 0.83 g/L reduces the photodegradation efficiency to 59.1 % or still lower. Therefore 0.50 g/L is the optimum catalyst loading for the given experimental condition.

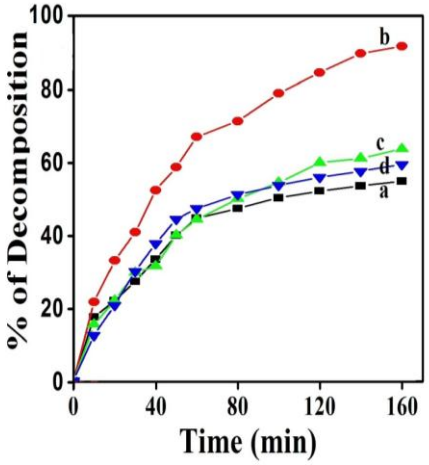

.

Fig. 11. Effect of catalyst dosage variation (g/L) in phenol photodegradation (a) 0.33, (b) 0.50, (c) 0.66 and (d) 0.83
Condition: pH = 4; [phenol] = 50 mg/L, Temp = 28±2°C and Fenton's reagent and constant air flow

Proposed Mechanism of phenol degradation

On the basis of the above experimental observations a possible mechanism has been proposed for photocatalytic oxidation of degradation of phenol with modified – Fenton's reagent in the presence of PANI-PTA-PVP catalyst, in equation (2)-(9).

$Fe^{+2} + H_2O_2 \longrightarrow Fe^{+3} + {\cdot}OH + OH^-$ ---------- (2)

${\cdot}OH + H_2O_2 \longrightarrow {\cdot}O_2H + H_2O$ ---------- (3)

$Fe^{+3} + {\cdot}O_2H \longrightarrow Fe^{+2} + O_2 + H^+$ ---------- (4)

$PANI\text{-}PTA\text{-}PVP + h\upsilon \longrightarrow h^+_{(VB)} + e^-_{(CB)}$ ---------- (5)

$H_2O_2 + 2h^+_{(VB)} \longrightarrow 2{\cdot}OH + O_2 + 2H^+$ ---------- (6)

$h^+_{(VB)} + H_2O \longrightarrow {\cdot}OH + H^+$ ---------- (7)

$e^-_{(CB)} + O_2 \longrightarrow O_2^{\cdot -}$ ---------- (8)

$Phenol + {\cdot}OH/\ O_2^{\cdot -}/\ {\cdot}O_2H \longrightarrow$ degradation products ---------- (9)

The ferrous ions decompose H_2O_2 into OH^- ion and ·OH radical, with the Fe^{+2} ions undergoing oxidation to Fe^{+3} ions. The reaction of ·OH with H_2O_2 produces $·O_2H$ radicals. The ferric ions are reduced to ferrous ions by $·O_2H$ radical and produce H^+ ions. Photocatalyst on exposure to light generate an electron-hole pair [40]. This hole may dissociate the H_2O_2 on the photocatalyst surface into oxygen, proton and $·O_2H$ whereas a hole may decompose H_2O into a proton and a hydroxyl radical. The electron reacts with oxygen into reactive, $O_2^{\cdot -}$ species. The reactive species (·OH/ $O_2^{\cdot -}$/ $·O_2H$) will degrade the phenol adsorbed on photocatalyst surface into degradation products. The phenol gets degraded into non-pollutant products.

CONCLUSION

Polyaniline and its composite photocatalysts, PANI–PVP, PANI–PTA and PANI–PTA–PVP have been successfully synthesized by a new green solvent (coconut oil) interfacial

polymerization method. Characterization by SEM revealed nanosticks/nanorods for PANI-PVP and surface-projected nanofriges/nanobristles structures on micron-size spherical particles for PANI-PTA and PANI-PTA-PVP composites. FTIR and XRD confirmed the presence of various components and their mutual interaction in PANI composites. On application to visible light degradation of phenol, the efficiencies of the four photocatalysts were in the above order. PANI-PTA-PVP exhibited the maximum efficiency of 86.2 % with H_2O_2 and 91.4 % with Fenton's reagent under optimal condition. Thus the new green solvent interfacial method produced nanostructured PANI composite photocatalysts with high efficiency in phenol photodegradation.

CONFLICT OF INTEREST

The authors declare that there is no conflict of interest.

REFERENCES

1. Loncar N, Bozic N, Andelkovic I, Milivanovic A, Dojnov B, Vujcic M, Roglic G, Vujcic Z. Removal of aqueous phenol and phenol derivatives by immobilized potato polyphenol oxidase. J Serb Chem Soc 2011; 76(4): 513-522.
2. Rubalcaba A, Suarez-Ojeda M E, Stuber F, Fortuny A, Bengoa C, Metcalfe I, Font J, Carrera J, Fabregat A. Phenol wastewater remediation: advanced oxidation processes coupled to a biological treatment. Water Sci Technol 2007; 55(12): 221-227.
3. Chang Q, Huang J, Ding Y, Tang H. Catalytic oxidation of phenol and 2,4-Dichlorophenol by using Horseradish peroxidase immobilized on Grephene oxide/ Fe_3O_4. Molecules 2016; 1044(21):1-10.
4. Singh S, Singh BB, Chandra R. Biodegradation of phenol in batch culture by pure and mixed strains of *Paenibacillus* sp. and *Bacillus cereus*. Pol J Microbiol 2009; 58(4): 319-325.
5. Opeolu BO, Fatoki OS, Odendaal J. Development of a solid-phase extraction method followed by HPLC-UV detection for the determination of phenols in water. Int J Phys Sci 2010; 5(5): 576-581.
6. Rao NN, Singh JR, Misra R, Nandy T. Liquid-liquid extraction of phenol from simulated sebacic acid waste water. J Sci Ind Res 2009; 68: 823-828.
7. Qadeer R, Rehan AH. A study of the adsorption of phenol by activated carbon from aqueous solutions. Turk J Chem 2002; 26: 357-361.
8. Nogueira RFP, Alberici RM, Mendes MA, Jardim WF, Eberlin MN. Photocatalytic degradation of phenol and trichloroethylene: On-line and Real-Time monitoring via membrane introduction Mass spectrometry. Ind Eng Chem Res 1999; 38: 1754-1758.
9. Dixit A, Mungray AK, Chakraborty M. Photochemical oxidation of phenol and chlorophenol by UV/H_2O_2/TiO_2 process: A kinetic study. Int J Comp Eng Appl 2010; 1(3): 247-250.
10. Devipriya SP, Yesodharan S. Photocatalytic degradation of phenol in water using TiO_2 and ZnO. J Env Biol 2010; 31: 247-249.
11. Thornton TD, Savage PE. Kinetics of phenol oxidation in supercritical water. AIChE J 1992; 38(3): 321-327.
12. Balachandran R, Patterson Z, Deymier P, Snyder SA. Understanding acoustic cavitation for sonolytic degradation of p-cresol as a model contaminant. Chemosphere 2016; 147: 52-59.
13. Joung-Eun Gu, Son G, Lee H, Park J, Young-Nam Kwon, Lee S. Improved water quality and phenol degradation via a combination of electron-beam irradiation (EBI) and activated carbon fiber(ACF). Desalin Water Treat 2017; 64: 118-126.
14. HE Feng, LEI Le-cheng., Degradation kinetics and mechanisms of phenol in photo-Fenton process. J Zhejiang Univ Sci 2004; 5(2): 198-205.
15. Male U, Srinivasan P, Singu BS. Incorporation of polyaniline nanofibres on graphene oxide by interfacial polymerization pathway for supercapacitor. Int Nano Lett 2015; 5: 231-240.
16. Li C, Zhang X, Wang K, Zhang H, Sun X, Ma Y. Dandelion-like cobalt hydroxide nanostructures: morphologiral evolution, soft template effect and super capacitive application. RSC Adv 2014; 4: 59603-59613.
17. Wang S, Chu L, Chen W. Fouling-resistant composite membranes for separation of Oil-in-water Microemulsions. Chinese J Chem Eng 2006; 14(1): 37-45.

18. Almedia JS, Jezur L, Fontana MC, Paese K, Silva CB, Pohilmann AR, Guterres SS, Beck RCR. Oil-based nanoparticles containing alternative vegetable oils (Grape seed oil and Almond kernel oil): Preparation and characterization. Lat Am J Pharm 2009; 28(2): 165-172.
19. Lowry OH, Rosebrough NJ, Farr AL, Randall RJ. Protein measurement with the Folin Phenol reagent. J Biol Chem 1951; 193: 265-275.
20. Zhang H, Li HX, Cheng HM. Water-soluble multiwalled carbon nanotubes functionalized with sulfonated polyaniline. J Phys Chem B 2006; 110: 9095-9099.
21. Murugesan R, Anitha G, Subramanian E. Multi-faceted role of blended poly (vinyl pyrrolidone) leading to remarkable improvement in characteristic of polyaniline emeraldine salt. Mater Chem Phys 2004; 85: 184-194.
22. Gong J, Xiu-Jun Cui, Ya-Guang Chen, Zhong-Wei Xie, Lun-Yu Qu. UV-Vis spectra of N, N'-Bis(4'-Aminophenyl)-1,4-quinonenediimine doped with $H_4SiW_{12}O_{40}$. Macromol Res 2004; 12(1): 22-25.
23. Marchena CL, Gomez S, Saux C, Pierella LB, Luis R Pizzio. Tungstophosphoric acid heterogenized onto NH_4ZSM_5 as an efficient and recyclable catalyst for the photocatalytic degradation of dyes. Quim Nova 2015; 38(4): 518-525.
24. Kanwal F, Siddiqi SA, Tasleem S, Sakina G, Tamil T. Synthesis and characterization of polyaniline/ wood and polyaniline/Carbon composites. Chem Soc Pak 2009; 31(6): 882-887.
25. Pecher J, Mecking S. Nanoparticles of conjugated polymers. Chem Rev 2010; 110: 6260-6279.
26. ALOthman ZA, Alam MM, Naushad M, Bushra R. Electrical conductivity and thermal stability studies on polyaniline Sn(IV) tungstomolybdate nanocomposite Cation-Exchange Material: Application as Pb(II) Ion-Selective membrane electrode. Int J Electrochem Sci 2015; 10: 2663-2684.
27. Subramanian E, Anitha G, Vijayakumar N. Constructive modification of conducting polyaniline characteristics in unusual proportion through nanomaterial blend formation with the neutral polymer Poly(vinyl pyrrolidone). J Appl Polym Sci 2007; 106: 673-683.
28. Popa A, Plesu N, Sasca V, Kis EE, Marinkovic-Neducin R. Physicochemical features of polyaniline supported heteropolyacids. J Optoelectron Adv M 2006; 8(5): 1944-1950.
29. Bandgar DK, Khuspe GD, Pawar RC, Lee CS, Patil VB. Facile and novel route for preparation of nanostructured polyanilien (PANi) thin films. Appl Nanosci 2014; 4: 27-36.
30. Gabal MA, Hussein MA, Hermas AA. Synthesis, characterization and electrical conductivity of polyaniline-$Mn_{0.8}Zn_{0.2}Fe_2O_4$ Nano-composites. Int J Electrochem Sci 2016; 11: 4526-4538.
31. Papagianni GG, Stergiou DV, Armatas GS, Kanatzidis MG, Prodromidis MI. Synthesis, characterization and performance of polyaniline-polyoxometalates (XM_{12}, X = P, Si and M = Mo, W) composites as electrocatalysts of bromates., Sensors Actuat B 2012; 173: 346-353.
32. Borji SH, Nasseri S, Mahvi AH, Nabizadeh R, Javadi AH. Investigation of photocatalytic degradation of phenol by Fe(III)- doped TiO_2 and TiO_2 nanoparticles. J Environ Health Sci Eng 2014; 12(101): 1-10.
33. Friedrich LC, de Paviva e Silva Zanta CL, Machulek A, de Oliveira Silva V, Quina FH. Interference of inorganic ions on phenol degradation by Fenton reaction. Sci Agric 2012; 69(6): 347-351.
34. Gomez H, Orellana F, Lizama H, Mansilla D, Dalclviele EA. Study of phenol Photodegradation with TiO_2/-WO_3 couple semiconductors activated by visible light. J Chil Chem Soc 2006; 51(4): 1006-1009.
35. Choquette-Labbe M, Shewa WA, Lalman JA, Shanmugam SR. Photocatalytic degradation of phenol and phenol derivatives using Nano-TiO_2 catalyst: integrating quantitative and qualitative factors using response surface methodology. Water 2014; 6:1785-1806.
36. Ahmed S, Rasul MG, Martens WN, Brown R, Hahib MA. Heterogeneous photocatalytic degradation of phenols in waste water: A review on current status and developments. Desalination 2010; 261(1-2): 3-18.

37. Bolobajev J, Kattel E, Viisimaa M, Goi A, Trapido M, Tenno T, Dulova N. Reuse of ferric sludge as an iron source for the Fenton-based process in wastewater treatment. Chemical Eng J 2014; 255: 8-13.
38. Bazaga-Garcia M, Cabeza A, Olivera-Pastor P, Santacruz I, Colodrero RMP, Aranda MAG. Photodegradation of phenol over a hybrid organo-inorganic material: Iron(II) hydroxyphosphonoacetate. J Phys Chem C 2012; 116: 14526-14533.
39. Cruz R, Reyes LH, Guzman-Mar Jorge L, Peralta-Hernandez JM, Hernandez-Ramirz A. Photocatalytic degradation of phenolic compounds contained in the effluent of a dye manufacturing industry. Sustain Environ Res 2011; 21(5): 307-312.
40. Sheikh MA, Kumar A, Paliwal M, Ameta R, Khandelwal RC. Degradation of organic effluents containing wastewater by photo-Fenton oxidation process. Indian J Chem Sec A 2008; 47A: 1681-1684.

Cite this article as:
P. Rajesh Anantha Selvan, E. Subramanian, R. Murugesan. New Green Solvent Interfacial Polymerization Method for Preparation of Nanostructured Polyaniline Composite Photocatalysts and Their Efficient Phenol Degradation With/Without Fenton's Reagent. J Pharm Chem Biol Sci 2017; 5(2): 133-146